Vibrational fingerprints of the Mn_4CaO_5 cluster in Photosystem II by mixed quantum-classical molecular dynamics

Daniele Bovi[†*], Matteo Capone[‡], Daniele Narzi[†], Leonardo Guidoni[†*]

[†] *Dept. of Physical and Chemical Science, University of L'Aquila, via Vetoio Coppito - 67100 L'Aquila, Italy*

[‡] *Dept. of Chemistry, University of Rome "La Sapienza", P.le Aldo Moro, 5, 00185 Roma, Italy*

Abstract

A detailed knowledge of the structures of the catalytic steps along the Kok-Joliot cycle of Photosystem II may help to understand the strategies adopted by this unique enzyme to achieve water oxidation. Vibrational spectroscopy have probed in the last decades the intermediate states of the catalytic cycle, although the interpretation of the data turned out to be often problematic. In the present work we use QM/MM molecular dynamics on the S_2 state to obtain the vibrational density of states at room temperature. To help the interpretation of the computational and experimental data we propose a decomposition of the Mn_4CaO_5 moiety into five separate parts, composed by "diamond" motifs involving four atoms. The spectral signatures arising by this analysis can be easier interpreted to assign experimentally known bands to specific molecular motions. In particular, we focussed in the low frequency region of the vibrational spectrum of the S_2 state. We can therefore identify the observed bands around 600-620 cm^{-1} as characteristic for the stretching vibrations involving Mn1-O1-Mn2 or Mn3-O5 moieties.

Keywords: Infrared Spectra, FTIR, Photosystem II, Density functional theory, VDOS

*Corresponding authors.

Email addresses: daniele.bovi@roma1.infn.it (Daniele Bovi[†]), leonardo.guidoni@univaq.it (Leonardo Guidoni[†])

1. Introduction

The water oxidation reaction occurring in the first steps of the natural photosynthesis is catalyzed by the protein/pigment complex Photosystem II (PSII). The active site of PSII consists of a cluster of four Mn and one Ca ions bound through μ-oxo-bridges [1]. The catalytic mechanism leading to the oxygen evolution proceeds through the five S_0-S_4 states of the Kok-Joliot's cycle [2, 3]. The characterization of the geometries as well as the electronic and magnetic properties specific for each step of the Kok-Joliot's cycle assumes a crucial importance in order to inspire scientists in developing manganese-based artificial devices able to fulfill with high efficiency the water oxidation reaction [4]. In this regard, important insights in the determination of the geometry of the different states of the catalytic cycle emerged in the last decades from X-ray crystallography [5, 6, 7, 1, 8] and from extended X-ray absorption fine structure experiments [9, 10, 11]. The electronic and magnetic properties of the active site of PSII along the Kok-Joliot's cycle were investigated by Electron Paramagnetic Spectroscopy (EPR), particularly focusing on the key step S_2 [12, 13, 14, 15, 16, 17, 18].

Combining the available experimental data with theoretical calculations it was possible characterize two possible isomers representative of the S_2 state [19, 20] (namely the open cubane S_2^A and the closed cubane S_2^B conformer) and suggest a path towards the S_3 state involving the transition between the two isomers [21, 22, 23]. The structure of the S_3 state was finally found to be consistent with a Mn_4Ca cluster arranged in a open cubane fashion [24, 25, 26, 27]. Although a large amount of experimental and theoretical data characterizing the five states of the Kok-Joliot cycle are now available, still the exact catalytic mechanism fulfilled by the Photosystem II remains elusive.

In the last decades Fourier Transform Infra Red (FTIR) vibrational spectroscopy was largely applied to investigate several states of the Kok-Joliot cycle of Photosystem II [28]. These studies allow to probe several aspect of the structural changes of the oxygen evolving complex along the catalytic cycle. FTIR difference spectra between different steps of the Kok-Joliot's cycle helped to identify which manganese ion undergoes oxidation during the S_n to S_{n+1} transition [29] and gave the possibility to determine the chemical properties of specific oxygen in the active site along the catalytic cycle [30, 31].

It has been investigated the network of the hydrogen bonds [32], the changes of the metal ligands [33, 28], the amide bands [34] and the influence of ions and amino-acids substitutions.

A critical point using vibrational spectroscopy consists of the assignment of the different bands to specific molecular vibration. In differential FTIR spectra applied to the study of large biological macromolecules, the contributions of the different moieties of the system to the spectrum make such assignment particularly complicated. In this respect, theoretical calculations provide a useful and efficient tool able to interprete the available experimental data, making the band assignment more reliable.

From the computational point of view, two main strategies have been developed. The first one consists of a normal mode analysis (NMA) which is done using a geometry-optimized zero-temperature conformer either in gas phase systems [35] or within a solvent that is usually described by a continuum medium [36]. The second strategy is based on linear-response theory. In this approach the FTIR spectra can be directly calculated from the dipole autocorrelation functions [37] obtained by an *ab initio* MD trajectory simulated at finite temperature. Unfortunately the resulting IR signal cannot be at present decomposed into the sums of independent signals and, on turn, its interpretation in terms of single vibrational modes is not easy. On the contrary, a clear interpretation and assignation of the vibrational peaks in term of independent collective motions, equivalents to the zero temperature normal modes is possible through a decomposition of the Vibrational Density of States (VDOS). The VDOS is also calculated from *ab initio* MD trajectories by computing the Fourier transform of the velocity autocorrelation function. To assign the vibrational signatures observed in the VDOS to specific molecular motions we can use the effective normal modes analysis (ENM) approach [39, 40]. The VDOS is decomposed into "effective normal modes" that include the effect of temperature, the anharmonicity of the potential, and, if present, the averaging between different conformers or hydrogen bonding networks along dynamics. Recent applications include the dynamics of the special pair of chlorophylls of PSII [38].

In the present work we performed *ab initio* molecular dynamics simulations coupled to Quantum Mechanics / Molecular Mechanics (QM/MM) scheme to describe the vibrational properties at finite temperature of the

catalytic cluster of Photosystem II in the S_2 state of the Kok-Joliot's cycle. To better identify the contribution of the Mn_4CaO_5 moiety to specific spectroscopic fingerprints we partitioned the cluster into 5 separated M_2O_2 diamonds (M = Mn, Ca). Thanks to this approach we can assign peaks in the low frequencies region from 350 to 700 cm^{-1} in which different studies performed on various organisms have tried to identified bands (reviewed in Ref.[41, 28]). In particular, anticipating our results, we can assign a band at 604/606 cm^{-1}, previously identified in the S_2 state [30, 31].

2. Methods

2.1. QM/MM system

The crystallographic structure of the oxygen-evolving Photosystem II at 1.9 Å resolution (PDB ID: 3ARC, [1]) was used as starting point of our calculations. The AMBER99SB force field [42] was used for describing the topology of the protein residues while the topologies of the other cofactors present in the structure were developed using the general AMBER force field (GAFF) [43] as described in Ref.[44]. A portion of the system consisting of the Mn_4CaO_5 cluster, the D1, D2 and CP43 protein domains,the cofactors and water molecules embedded in such region was used for the QM/MM calculations. Starting positions of the atoms belonging to the Mn_4CaO_5 cluster and the four directly bound water molecules in the S_2 state were taken by Patanzis *et al.* [19] considering both open closed-cubane isomers (namely S_2^A and S_2^B models). The region treated at DFT level consists of the Mn_4CaO_5 cluster, its ligands (Asp170, Glu189, His332, Glu333, Asp342, Ala344, and CP43-Glu354), the closest residues (Asp61, Tyr161, His190, His337, Ser169 and CP43-Arg357), and the four water molecules directly bound to the metal cluster, consistently with previous calculations [44, 45]. Ten additional water molecules close to the cluster as well as the chloride anion close to Glu333 were also treated at DFT level. The rest of the system was described by the classical force field. The QM/MM calculations were carried out using the CP2K package in a mixed quantum/classical approach [46]. The electrostatic coupling between the the classical and the quantum region of the system was treated by means of fast gaussian expansion of the electrostatic potential [47].

The QM/MM molecular dynamics (MD) simulations were carried out in NVT ensemble. The system was coupled with a thermal bath at 298K using

the Nosé-Hoover thermostat [48, 49, 50] with a time constant of 0.1 ps. The QM region was treated in a cubic cell with dimensions 28.0 28.0 28.0 Åand a cutoff for the plane-wave expansion set to 320 Rydberg. QM/MM MD simulations were carried out with a time step of 0.5 fs for at least 10 ps plus 3 ps of equilibration. The PBE+U scheme [51, 52, 53] was adopted for the QM region as described in Ref.[44] using the DZVP-MOLOPT-SR-GTH Gaussian basis set optimized for molecular systems [54]. Coordinates of the C_α atoms were fixed in the starting positions during the dynamic. The ground spin states (total spin S = 1/2 for S_2^A and S = 5/2 for S_2^B) were considered for the two simulated systems consistently with previous works [19, 20].

2.2. Vibrational Analysis

The vibrational density of states (VDOS) were directly obtained from the QM/MM MD simulations:

$$\mathrm{P}(\omega) = \sum_{i=1}^{N} \int_{-\infty}^{\infty} dt \, \left\langle \vec{\mathrm{r}}_i(t) \cdot \vec{\mathrm{r}}_i(0) \right\rangle \exp\left(i\omega t\right) = \sum_{i=1}^{N} \mathrm{P}_i^{\mathrm{r}}(\omega) = \sum_{k=1}^{3N-6} \mathrm{P}_k^{\mathrm{q}}(\omega) \quad (1)$$

where $\mathrm{P}_i^{\mathrm{r}}$ is the VDOS for the i-th atom of the system (N atoms) in the position $\vec{r}_i$. This allows to determine each atomic contribution to the vibrational spectrum [40].

The normal modes analysis can be extended with a finite temperature formulation [39], introducing a linear transformation from the internal variables of the molecule $(3N-6)$ to generalized coordinate q_k which represents the finite temperature analogues of the normal modes. The total VDOS can be decomposed into a sum of $(3N-6)$ spectral terms, $\mathrm{P}_k^{\mathrm{q}}(\omega)$ (VDOS of the transformed coordinate q_k, eq. 1), obtained by minimizing the functional $\Omega^{(n)}$ (eq. 2) with respect the choice of set $\{q_k\}$, characterized by a single peak shape around the frequency ω_k.

$$\Omega^{(n)} = \sum_k \left[\frac{\beta}{2\pi} \int_{-\infty}^{\infty} d\omega |\omega^{2n}| P_k^q(\omega) \; - \left(\frac{\beta}{2\pi} \int_{-\infty}^{\infty} d\omega |\omega^n| P_k^q(\omega) \right)^2 \right] \quad (2)$$

The set of coordinates q_k, namely Effective Normal Modes, therefore describe the collective motions around the frequency ω_k. In eq. 2 the standard value $n = 2$ was used, thus allowing to replace the minimization problem by

a generalized eigenvalue problem [39, 40].

In this paper we would like to focus on the vibrational signatures of the Mn_4CaO_5 cluster core. To this purpose our intent is to deeply analyze and characterize the dynamics of these 10 atoms. To this aim, the VDOS of the Mn_4CaO_5 subset of atoms were partitioned in diamond subunits of 4 atoms each, as shown in Fig. 3 and 4). Although this partitioning is redundant, the contribution of each diamond can provide a good interpretation of the major features of the spectra and may help to assign localized vibrational modes. Within each M_2O_2 (M=Mn,Ca) diamond we subsequently applied the effective normal modes analysis, obtaining the contribution of specific molecular motion (such bonding, angle, dihedral) to the VDOS spectra. In particular we focussed on the Mn-O stretching region of the spectra, which is composed in both open and closed conformer by 11 Mn-O bonds. On the basis of the results obtained through the potential energy decomposition of the effective normal modes [55] we have therefore assigned a specific combination of stretching modes to each of the 11 frequencies in the stretching region of the spectra. Although normal modes are in general delocalized in space we have tried to provide, when possible, a localized picture such modes, indicating in Table 1 only the stretching motions which more significantly contribute to each frequency. Due to the redundancy of the diamond decomposition, a single frequency may appear in adjacent diamonds. In this case we have indicated the mode which are less mixed in term of PED contributions and more localized in frequency. We are aware of the degrees of arbitrariness intrinsic in such assignments, but we believe that this procedure is rather robust and it can pinpoints specific and localized features useful to interpret the experimental data.

3. Results and Discussion

In the present work we carried out QM/MM molecular dynamics simulations of the catalytic core of the Photosystem II in two different conformations characteristic of the S_2 state of the Kok-Joliot cycle, namely the S_2^A open cubane conformer, responsible for the multiline EPR singal and the closed S_2^B conformer, responsible for the g=4.1 EPR signal.[19] On both models vibrational density of states spectra were calculated from the two 10 ps long equilibrated trajectories. The assignment of vibrational signatures in

the low frequency region of the Mn_4CaO_5 core to specific vibrational modes is therefore discussed.

3.1. Total spectrum Model-A

The Vibrational density of states spectrum for the S_2^A open cubane conformer was calculated taking into account the trajectory of the whole quantum region (206 atoms) and reported in Fig. 2. We point out that the S_2^A open cubane state was found to be thermodynamically more stable with respect to the S_2^B closed state at environmental temperature [20]. It therefore represents the conformer most populated at physiological conditions. In addition, at lower temperature, the Boltzmann population of the more stable isomer will increase. Therefore, experimental FTIR studies on the S_2 state of the Kok-Joliot's cycle should be compared with the outcomes obtained from the simulation of the S_2^A state only.

The VDOS spectrum for the S_2^A state is reported in the upper panel of the Fig.2 in the frequency range between 350 cm^{-1} and 1850 cm^{-1} in which is concentrated the fingerprints of the Mn-cluster and its ligands. Additionally, in order to identify the contributions of different moieties of the system, the VDOS spectrum was also calculated on restricted sets of atoms. In particular, as illustrative examples, we have shown in Fig.2 the contribution of different moieties to the VDOS spectra: the Mn_4CaO_5 cluster, some selected amino acids, the carboxylate ligands (only the atoms belonging to the COO^- binding groups) and the water molecules. In the second panel the carboxylate ligands are shown divided between: those bridging two manganese ions, those bridging one manganese and one calcium cation and the monodetate lignad to one manganese ion. In the third panel are shown the active residues close to the manganese cluster: His332, Asp61 and the Tyr161/His190 moiety. Finally, in the fourth panel, the VDOS spectra of the water molecules bound to the Mn_4CaO_5 cluster (divided between those binding the calcium and those binding the Mn ion) are reported.

As highlighted in the second panel of the Fig.2 the region corresponding to the vibrations of the Mn_4CaO_5 cluster was found to be mainly localized between 350 cm^{-1} and 650 cm^{-1} in agreement with previous experimental FTIR studies [30, 31, 28]. Assignments of the bands to the different vibrational modes of the Mn_4CaO_5 cluster will be described in the next section and it is the main focus of the present paper. Apart from the manganese cluster,

comparing the VDOS calculated on the His332 side chain (pink curve) and the VDOS of the Tyr-Z-His190 moiety (brown curve), we can observe several characteristic peaks at different frequencies (third panel Fig.2). In particular the peak at $\sim$1115 cm^{-1} can be assigned to the characteristic CN stretching band of the imidazole group of both the His190 and His332. This band was previously suggested to identify the His structure and being sensitive to the protonation state of the histidine [56, 57, 58, 59]. It has to be pointed out that both the above mentioned histidines are singularly protonated during the simulation. Peaks at $\sim$1610 cm^{-1} and $\sim$1500-1520 cm^{-1} were found only for the Tyr-Z-His190 group and not for the His332. The band at $\sim$1610 cm^{-1} could be assigned to the ring modes of the tyrosine residue, as suggested in ref. [60].

Symmetric and asymmetric carboxylate stretching regions are typically found at 1300-1450 and 1500-1600 cm^{-1} [59]. While the assignment of the bands corresponding to the symmetric stretching is more straightforward, due to the absence of other overlapping bands, in the case of the asymmetric stretching the situation is more complicated. Indeed, in the region at 1500-1600 cm^{-1} the amide II bands strongly overlap with the asymmetric carboxylate bands, thus making difficult the assignment of such bands. In our calculations, taking into account only the trajectory of the carboxylate groups directly coordinated with the Mn_4CaO_5 cluster, we obtained the peculiar spectrum of those ligands. We further divided such moieties in three groups, the first with the bidentate carboxyl groups binding two Mn ions (red line, second panel Fig.2), the second with bidentate groups bridging one Mn and one Ca ion (green line, second panel Fig.2), the last with the monodentate Mn ligand (dark-yellow line, second panel Fig.2). In this way we can easier identify which kind of moieties mostly contributes to a specific band.

Our results show more localized bands and lower frequencies for the three Mn_2 ligands with a sharp peak at $\sim$1510 cm^{-1} correspondig to the asymmetric stretching. The two etero-ions ligands decomposed spectra show a wider active region with two sharp peaks at $\sim$1490 and $\sim$1580 cm^{-1}. The last selection with only one monodetate ligand shows the asymmetric stretching peak at $\sim$1620 cm^{-1}. The other regions rich in vibrational density are not considered for this study. Those peaks come out from the closest interaction of the COO^- group, bringing into the spectra vibrational mode typical of the manganese cluster.

Moreover, we can restrict the calculation to the side chain of a single residue and from its VDOS we can assign the bands to specific vibrational

modes, as we did in the case of Asp61 (orange line, third panel Fig.2). For Asp61, our calculations show the presence of two bands at $\sim$ 1350 cm^{-1} and at $\sim$ 1565 cm^{-1}, falling in the regions corresponding to the (de-protonated) carboxylate stretching, always present in the typical fingerprint of caboxylate group infrared adsorption, and assigned respectively to the symmetric stretching and asymmetric stretching.

In the bottom panel of Fig. 2 the decomposed VDOS of the water ligands of the Mn_4CaO_5 cluster are reported. The four water molecules were divided based on kind of binding metal. As shown in the figure, most of the changing appears between $\sim$1500-1850cm^{-1}, in the bending mode region. The VDOS of the two H_2O molecules bound to a Ca ion (light-blue line, bottom panel of Fig.2) is in the same spectral region as the COO^- ligands, whereas for the water molecule and the OH^- group bound to the Mn4 ion (purple line, bottom panel of Fig.2) the band is much more localized around 1600 cm^{-1}. To better identify such region it will be necessary in the future to consider differences occurring between S_2 and other states of the Kok-Joliot cycle.

Overall, the calculation of the VDOS relative to the H_2O / OH^- groups directly bound to the Mn_4CaO_5 cluster, reported in the lower panel of Fig.2, could turn out a valuable tool in combination with experimental differential FTIR spectra in order to determine the identity of the substrate water molecule, thus helping to elucidate the water binding mechanism.

A systematic and comprehensive description of the calculated vibrational spectra is beyond the purpose of the present work, which is focused on the description of the vibrational modes of the Mn_4CaO_5 cluster (see next section). Nevertheless, the results reported in this work represent a first step towards the interpretation of FTIR spectra of a highly complex system such as the oxygen evolving complex of Photosystem II.

3.2. Model-A: Open Cubane structure

The open cubane structure represents the most stable conformer in the S_2 state [19, 20] and therefore the available FTIR spectra of the S_2 state should be mainly representative of such conformer. In this section we analyze the VDOS associated with the Mn_4CaO_5 cluster whitin the QM/MM MD trajectory of the open cubane S_2 state. As shown in Fig. 3 we have considered the open cubane cluster as composed by five diamonds formed by four atoms. Internal coordinates (namely, bond stretching, diamond deformation and diamond puckering) has been defined for each one of these 4-member ring , as

recommended by Pulay *et al.* [61]. The frequencies region described (350-750 cm^{-1}) is well recognized as typical infrared fingerprint for the Mn_4CaO_5 cluster. Considering that all motions involve vibrations of Mn and oxo ions, we can therefore reasonably assume that each vibrational mode described by our diamond decomposition and normal mode analysis is IR active.

As shown in the upper panel of Figure 3, the VDOS contribution of the four rings clearly indicates that different diamonds has different fingerprints. Some of the peak can be clearly assigned to one diamond only, whereas others comes from the contribution of more then one diamond. The contribution of each diamond has been further decomposed by means of effective normal mode analysis, as shown in the lower panel of Figure 3. The nature of the contribution to specific peaks can be extracted through the potential energy distribution analysis [40]. Smaller frequency motions, involving Ca-O stretching and angle bending, turned out to be of mixed nature and not well-defined, also due to the limited sampling of dynamics. Higher frequency motions, which are Mn-μ-oxo bond stretching, are better characterized, although they were found to be localized in a rather broad frequency region between 414 cm^{-1} and 647 cm^{-1} as reported in Tab. 1. We have to point out that the 5 diamonds share some of the Mn-O bonds, therefore the decomposition is intrinsically redundant and the same peak may appear in different diamonds. Nevertheless, we have tried to assign the 11 Mn-O frequencies to modes which are as much localized in space as possible as reported in Figure 1. Diamond 1 and Diamond 4 defined in Fig.3, showed a clear band around 600-620 cm^{-1}. Such band involves two stretching for the Diamond 1 (for the Mn1-O1-Mn2 and the Mn2-O1 moieties at 617 and 604 cm^{-1} respectively). The Diamond 4 contributes to such band with the Mn2-O2 moiety (600 cm^{-1}). The same band is also present in Diamond 2, albeit less intense. Other significant bands for which the assignment is very clear are: the bands coupled with the Diamond 3 motions, at 647 cm^{-1} (stretching of Mn3-O4) and at 477 cm^{-1} (asymmetric stretching of O4-Mn4-O5); the band coupled with the Diamond 5 motions, at 594 cm^{-1} (stretching of Mn3-O5) and the band coupled with the Diamond 1 at 524 and 495 cm^{-1} (symmetric and asymmetric stretching of Mn1-O3-Mn2).

Using differential FTIR spectroscopy, one particular positive band at 604[62] or 606[30] cm^{-1}(depending on the organism) in the S_2-*minus*-S_1 has been extensively discussed in the literature[30, 63, 64, 28, 65]. This band can

be either eliminated or shifted to 623 cm^{-1} in presence of ammonia [63]. Additionally, it is downshifted to 596 cm^{-1} in presence of $H_2{}^{18}O$, thus revealing the exchange of the water with an oxo-bridge [30]. Based on these results as well as FTIR spectra on mutated systems [65], it was suggested that the μ-oxo atom in the Mn-O-Mn moiety responsible for the vibrational mode at 604/606 cm^{-1} is a substrate oxygen, tentatively assigned to the O5 μ-oxo [64, 28].

When comparing the DFT results with the experimental spectra we need to keep in mind that different functionals and other computational details may affect the absolute value of the frequencies which are usually within a 5% range. On the other side, the relative shift between computed vibrational frequency is more robust and less conditioned by the computational details. If we keep this in mind we can conclude that our calculations identify three bands which fall in the range 570/620 cm^{-1} which may correspond to the experimentally determined band at 604/606 cm^{-1}: a band at 617 cm^{-1} corresponding to the Mn1-O1-Mn2 asymmetric vibrational mode, a band at 604 cm^{-1} corresponding to the Mn2-O1 vibrational mode, a band at 600 cm^{-1} due to the stretching of Mn2-O2 and a band at 594 $cm^{-}1$ due to the stretching of Mn3-O5 vibrational mode.

Despite it is not possible to assign unambiguously the experimental band at 604/606 cm^{-1} to one of the above vibrational modes, our results restricts the possible interpretations, limiting the assignment to two different possibilities.

A first interpretation is that such band originates from the characteristic angle bending vibrations around Mn2 in the S_2 state. Despite the fact that ammonia and the $H_2{}^{18}O$ can exchange with the O5 μ-oxo with the consequent elimination or modification of the band at 604/606 cm^{-1}, this could not necessarily imply an assignation of such band to a stretching involving the O5 μ-oxo itself. A second possibility is that the band involves directly the Mn3-O5 stretching, as previously suggested [41].
It is interesting to note that this second interpretation is pointing towards the O5 μ-oxo, which seems to have a special role in the S_2 state, where its position regulates the interconversion between the two different open and closed conformers [19, 20]. Such condition is probably a characteristic of the S_2 state and might be a fingerprint of the S_2 spectra which is not present in the S_1 and S_3 spectra.

As it will be shown in the next section a perturbation of the cluster involving the O5 atom turns out not only in a modification of the band assigned

to vibrational modes involving directly the μ-oxo O5, but also a modification of the other bands assigned to different vibrational modes.

In addition, from Fourier transform infrared difference spectra between the S_2 and the S_1 state in the PSII of the *Thermosynechococcus elongatus*, it was possible identify several other positive bands at 430, 471, 546, 590, 604, 629, 642, and 660 cm^{-1} [31]. Albeit, as mentioned before, we are not able to determine with high accuracy the exact frequency of these motions, it is worth to notice the good overlap between the calculated frequencies and part of the experimentally determined bands characteristic of the S_2 state.

3.3. Model-B: Closed Cubane structure

Although, as previously discussed, the S_2^A model is more stable than the S_2^B model at physiological conditions, the comparison between the two conformers can be indeed useful to identify specific fingerprints of the closed and open conformers that might be potentially relevant for other states along the Kok-Joliot cycle or for studies in non-physiological conditions. The effective normal modes analysis was additionally carried out on the QM/MM trajectory of the closed cubane S_2^B model. The structural differences between such model and the most stable S_2^A model mainly reside on the different position of the O5 atom that induces a change in the different spin ground state (S=1/2 and S=5/2 for the S_2^A and S_2^B model respectively). The comparison of the two spectra pointed out that there are quite significant changes and shifts of many of the characteristic bands. In particular for the diamond 1 equally defined in both models (Mn1-O1-Mn2-O3), the main band between 600 and 620 cm^{-1} found in the open cubane model, was found to be slightly red shifted by approximately $\sim$10 cm^{-1}. As in the case of diamond 1, also the diamond 4 is equally defined in both the S_2 isomers (Ca-O1-Mn2-O2). The characteristic band found around 600 cm^{-1} in the open cubane model and assigned to the stretching of the Mn2-O2 moiety is blue shifted at $\sim$626 cm^{-1} in the closed cubane conformer. Finally, in the S_2^B model an additional moiety not present in the S_2^A model, namely the hook consisting of the Mn3-O4-Mn4 atoms, can be defined. Such structural difference lead to the appearing of bands at wavelengths in the 700-750 cm^{-1} region, which is typical for singly oxo-bridged Mn clusters and it was not present in the VDOS spectrum of the open cubane S_2^A conformer. In particular the 696 cm^{-1} peak in the S_2^B spectra corresponds to the Mn3-O4 stretching, which was at 647 cm^{-1} in the

open cubane S_2^A.

We remind again that the results obtained from the analysis of the closed cubane S_2^B conformer cannot be directly compared with the available experimental data since its lower stability with respect to the open cubane S_2^B conformer makes the vibrational modes not detectable in the experimental conditions. Nevertheless, our results clearly show that a modification in the position of the O5 has also a large impact on the vibrational modes of the other moieties of the Mn_4CaO_5 cluster.

4. Conclusions

Fourier transform infrared difference spectroscopy turned out in the last decades as a valuable and efficient tool to investigate structural changes occurring in the active site of the Photosystem II along the Kok-Joliot's cycle. One limit of such technique consists of the intrinsic difficulty in univocally assign a given band to the respective vibrational mode. In this regard theoretical calculations might help to interprete experimental data, providing with a framework in which the band assignment can be validated. In the present work, we have calculated through QM/MM molecular dynamics, the vibrational density of states of the Mn_4CaO_5 cluster of PSII in the S_2 state, laying the foundation for a rationale interpretation of the FTIR spectra. We have focussed our analysis on The Mn-O stretching region, which covers a wide range, from 400 and 700 cm^{-1}. To facilitate the interpretation of the spectra we have decomposed the Mn_4CaO_5 structure into different diamonds, and used the effective normal mode analysis to characterize their internal motions. The 11 stretching frequencies were identified and specific, localized, stretching modes were attributed.

We have also attempt to assign the well-identified band at 604/606 cm^{-1} [62, 30] which was experimentally determined by FTIR difference spectroscopy in the low frequency region for the S_2-*minus*-S_1 spectrum, and previously assigned to a Mn-O-Mn vibrational mode involving the μ-oxo O5 [64, 28, 41]. Our data suggest two possibilities: it could arise from the Mn3-O5 stretching (calculated band at 594 cm^{-1}) or from the Mn2 vibrational mode with O1 (calculated band at 604 cm^{-1}) or with O2 (calculated band at 607 cm^{-1}).

The comparison between the spectra in the open and closed conformations shows a significant rearrangement of many Mn-O stretching bands between the two conformers, indicating that a change in O5 position should have

a rather important effect on the IR spectra. Since the FTIR data report that between S_1 and S_3 there are no dramatic changes in that region of the spectra, this fact may represent a further evidence that all the S_1, S_2 and S_3 states share the same, open cubane, conformer.

A step forward in the interpretation of the experimental spectra by using the theoretical approach here employed would consists in the extension of the calculations to other molecular models along the Kok-Joliot's cycle. The computing of differences between the power spectra of several models may indeed help to identify the observed bands determined by FTIR difference spectroscopy.

Acknowledgements

The authors acknowledge PRACE infrastructure and the Caliban-HPC centre at the University of L'Aquila for the computational resources supplied. Funds were provided by the European Research Council project n. 240624 within the VII Framework Program of the European Union.

References

[1] Y. Umena, K. Kawakami, J.-R. Shen, N. Kamiya, Crystal structure of oxygen-evolving photosystem II at a resolution of 1.9 angstrom, Nature 473 (2011) 55–65.

[2] B. Kok, B. Forbush, M. McGloin, Cooperation of charges in photosynthetic O2 evolution, Photochem. Photobiol. 11 (1970) 457–475.

[3] P. Joliot, B. Kok, Oxygen evolution in photosynthesis, Bioenergetics of photosxynthesis (1975) 387–412.

[4] T. Faunce, S. Styring, M. R. Wasielewski, G. W. Brudvig, A. W. Rutherford, J. Messinger, A. F. Lee, C. L. Hill, H. deGroot, M. Fontecave, D. R. MacFarlane, B. Hankamer, D. G. Nocera, D. M. Tiede, H. Dau, W. Hillier, L. Wang, R. Amal, Artificial photosynthesis as a frontier technology for energy sustainability, Energy Envir. Sci. 6 (2013) 1074–1076.

[5] A. Zouni, H. T. Witt, J. Kern, P. Fromme, N. Krauss, W. Saenger, P. Orth, Crystal structure of photosystem II from Synechococcus elongatus at 3.8 Åresolution, Nature 409 (2001) 739–743.

[6] B. Loll, J. Kern, W. Saenger, A. Zouni, B. J, Towards complete cofactor arrangement in the 3.0 Åresolution structure of photosystem II, Nature 438 (2005) 1040–1044.

[7] A. Guskov, J. Kern, A. Gabdulkhakov, M. Broser, A. Zouni, S. W, Cyanobacterial photosystem II at 2.9 Åresolution and the role of quinones, lipids, channels and chloride, Nat. Struct. Mol. Biol. 16 (2009) 334–342.

[8] M. Suga, F. Akita, K. Hirata, G. Ueno, H. Murakami, Y. Nakajima, T. Shimizu, K. Yamashita, M. Yamamoto, H. Ago, J.-R. Shen, Native structure of photosystem II at 1.95 Å resolution viewed by femtosecond X-ray pulses, Nature 517 (2014) 99–103.

[9] J. H. Robblee, R. M. Cinco, Y. V. K, X-ray spectroscopy-based structure of the Mn cluster and mechanism of photosynthetic oxygen evolution, Biochim. Biophys. Acta Bioenerg. 1503 (2001) 7–23.

[10] J. Yano, J. Kern, K. Sauer, M. J. Latimer, Y. Pushkar, J. Biesiadka, B. Loll, W. Saenger, J. Messinger, A. Zouni, Y. V. K, Where water is oxidized to dioxygen: structure of the photosynthetic Mn_4Ca cluster, Science 314 (2006) 821–825.

[11] H. Dau, A. Grundmeier, P. Loja, M. Haumann, On the structure of the manganese complex of photosystem II: extended-range EXAFS data and specific atomic-resolution models for four S-states, Phil. Trans. Royal Soc. B - Biol. Sci. 363 (2008) 1237–1243.

[12] G. C. Dismukes, S. Y, Intermediates of a polynuclear manganese center involved in photosynthetic oxidation of water, Proc. Nat. Acad. Sci. USA 78 (1981) 274–278.

[13] J. L. Casey, S. K, EPR detection of a cryogenically photogenerated intermediate in photosynthetic oxygen evolution, Biochim. Biophys. Acta Bioenerg. 767 (1984) 21–28.

[14] J. C. De Paula, J. B. Innes, G. W. Brudvig, Electron transfer in photosystem II at cryogenic temperatures, Biochemistry 24 (1985) 8114–8120.

[15] A. Boussac, J.-J. Girerd, A. W. Rutherford, Conversion of the Spin State of the Manganese Complex in Photosystem II Induced by Near-Infrared Light, Biochemistry 35 (1996) 6984–6989.

[16] A. Boussac, S. Un, O. Horner, A. W. Rutherford, High-Spin States ($S \geq 5/2$) of the Photosystem II Manganese Complex, Biochemistry 37 (1998) 4001–4007.

[17] J. H. Su, N. Cox, W. Ames, D. A. Pantazis, L. Rapatskiy, T. Lohmiller, L. V. Kulik, P. Dorlet, A. W. Rutherford, F. Neese, A. Boussac, W. Lubitz, J. Messinger, The electronic structures of the S-2 states of the oxygen-evolving complexes of photosystem II in plants and cyanobacteria in the presence and absence of methanol, Biochim. Biophys. Acta 107 (2011) 829–840.

[18] J. Sjöholm, S. Styring, K. G. V. Havelius, F. M. Ho, Visible Light Induction of an Electron Paramagnetic Resonance Split Signal in Photosystem II in the S_2 State Reveals the Importance of Charges in the Oxygen-Evolving Center during Catalysis: A Unifying Model, Biochemistry 51 (2012) 2054–2064.

[19] D. A. Pantazis, W. Ames, N. Cox, W. Lubitz, F. Neese, Two Interconvertible Structures that Explain the Spectroscopic Properties of the Oxygen-Evolving Complex of Photosystem II in the S2 State, Ang. Chem. Int. Ed. 51 (2012) 9935–9940.

[20] D. Bovi, D. Narzi, L. Guidoni, The S_2 State of the OxygenEvolving Complex of Photosystem II Explored by QM/MM Dynamics: Spin Surfaces and Metastable States Suggest a Reaction Path Towards the S_3 State , Ang. Chem. Int. Ed. 52 (2013) 11744–11749.

[21] N. Cox, J. Messinger, Reflections on substrate water and dioxygen formation, Biochim. Biophys. Acta Bioenerg. 1827 (2013) 1020–1030.

[22] D. Narzi, D. Bovi, L. Guidoni, Pathway for Mn-cluster oxidation by tyrosine-Z in the S_2 state of photosystem II, Proc. Natl. Acad. Sci. USA 111 (2014) 8723–8728.

[23] A. Boussac, A. W. Rutherford, M. Sugiura, Electron transfer pathways from the s_2-states to the s_3-states either after a ca^{2+}/sr^{2+} or a cl^-/i^- exchange in photosystem ii from thermosynechococcus elongatus, Biochim. Biophys. Acta Bioenerg. 1847 (2015) 576–586.

[24] P. E. M. Siegbahn, Water oxidation mechanism in photosystem II, including oxidations, proton release pathways, O-O bond formation and O_2 release, Biochim. Biophys. Acta Bioenerg. 1827 (2013) 1003–1019.

[25] N. Cox, M. Retegan, F. Neese, D. A. Pantazis, A. Boussac, W. Lubitz, Electronic structure of the oxygen-evolving complex in photosystem ii prior to o-o bond formation, Science 345 (6198) (2014) 804–808.

[26] M. Capone, D. Bovi, D. Narzi, L. Guidoni, Reorganization of Substrate Waters between the Closed and Open Cubane Conformers during the S_2 to S_3 Transition in the Oxygen Evolving Complex, Biochemistry 54 (2015) 6439–6442.

[27] M. Capone, D. Narzi, D. Bovi, L. Guidoni, Mechanism of Water Delivery to the Active Site of Photosystem II along the S_2 to S_3 Transition, J. Phys. Chem. Lett. 7 (2016) 592–596.

[28] R. J. Debus, FTIR studies of metal ligands, networks of hydrogen bonds, and water molecules near the active site Mn4CaO5 cluster in Photosystem II, Biochim. Biophys. Acta-Bioenergetics 1847 (2015) 19–34.

[29] M. A. Strickler, L. M. Walker, W. Hillier, R. D. Britt, R. J. Debus, No Evidence from FTIR Difference Spectroscopy that Aspartate-342 of the D1 Polypeptide Ligates a Mn ion that Undergoes Oxidation during the S_0 to S_1, S_1 to S_2, or S_2 to S_3 Transitions in Photosystem II, Biochemistry 46 (2007) 3151–3160.

[30] H. A. Chu, H. Sackett, G. T. Babcock, Identification of a Mn-O-Mn cluster vibrational mode of the oxygen-evolving complex in photosystem II by low-frequency FTIR spectroscopy, Biochemistry 39 (2000) 14371–14376.

[31] Y. Kimura, A. Ishii, T. Yamanari, T.-a. Ono, Water-Sensitive Low-Frequency Vibrations of Reaction Intermediates during S-State Cycling in Photosynthetic Water Oxidation , Biochemistry 44 (2005) 7613–7622.

[32] T. Noguchi, M. Sugiura, FTIR Detection of Water Reactions during the Flash-Induced S-State Cycle of the Photosynthetic Water-Oxidizing Complex, Biochemistry 41 (2002) 15706–15712.

[33] R. J. Debus, Evidence from FTIR Difference Spectroscopy That D1-Asp61 Influences the Water Reactions of the Oxygen-Evolving Mn4CaO5 Cluster of Photosystem II, Biochemistry 53 (2014) 2941–2955.

[34] Y. Kimura, N. Mizusawa, A. Ishii, T. Yamanari, T.-a. Ono, Changes of Low-Frequency Vibrational Modes Induced by Universal ^{15}N- and ^{13}C-Isotope Labeling in S_2/S_1 FTIR Difference Spectrum of Oxygen-Evolving Complex, Biochemistry 42 (2003) 13170–13177.

[35] E. Gloaguen, B. de Courcy, J. Piquemal, J. Pilme, O. Parisel, R. Pollet, H. Biswal, F. Piuzzi, B. Tardivel, M. Broquier, M. Mons, Gas-phase folding of a two-residue model peptide chain: On the importance of an interplay between experiment and theory, J. Am. Chem. Soc. 132 (2010) 11860–11863.

[36] N. Kausar, T. J. Dines, B. Z. Chowdhry, B. D. Alexander, Vibrational spectroscopy and DFT calculations of the di-amino acid peptide l-aspartyl-l-glutamic acid in the zwitterionic state, Phys. Chem. Chem. Phys. 11 (2009) 6389–6400.

[37] M.-P. Gaigeot, Theoretical spectroscopy of floppy peptides at room temperature. a DFTMD perspective: gas and aqueous phase, Phys. Chem. Chem. Phys. 12 (2010) 3336–3359.

[38] D. Narzi, D. Bovi, P. De Gaetano, L. Guidoni, Dynamics of the Special Pair of Chlorophylls of Photosystem II, J. Am. Chem. Soc. 138 (2016) 257–264.

[39] M. Martinez, M.-P. Gaigeot, D. Borgis, R. Vuilleumier, Extracting effective normal modes from equilibrium dynamics at finite temperature, J. Chem. Phys. 125 (2006) 144106.

[40] M.-P. Gaigeot, M. Martinez, R. Vuilleumier, Infrared spectroscopy in the gas and liquid phase from first principle molecular dynamics simulations: application to small peptides, Mol. Phys. 105 (2007) 2857–2878.

[41] H.-A. Chu, Fourier transform infrared difference spectroscopy for studying the molecular mechanism of photosynthetic water oxidation, Front. Plant Sci. 4 (2013) 1–6.

[42] V. Hornak, R. Abel, A. Okur, B. Strockbine, A. Roitberg, C. Simmerling, Comparison of multiple amber force fields and development of improved protein backbone parameters, Proteins 65 (2006) 712–725.

[43] J. Wang, R. M. Wolf, J. W. Caldwell, P. A. Kollman, D. A. Case, Development and testing of a general amber force field, J. Comput. Chem. 25 (2004) 1157–1174.

[44] D. Bovi, D. Narzi, L. Guidoni, Magnetic interactions in the catalyst used by nature to split water: a DFT+U multiscale study on the Mn_4CaO_5 core in Photosystem II, New J. Phys. 16 (2014) 015020.

[45] F. Pitari, D. Bovi, D. Narzi, L. Guidoni, Characterization of the Sr^{2+}- and Cd^{2+}-Substituted Oxygen-Evolving Complex of Photosystem II by Quantum Mechanics/Molecular Mechanics Calculations, Biochemistry 54 (38) (2015) 5959–5968.

[46] T. Laino, F. Mohamed, A. Laio, M. Parrinello, An efficient real space multigrid QM/MM electrostatic coupling, J. Chem. Theory Comput. 1 (2005) 1176–1184.

[47] J. VandeVondele, M. Krack, F. Mohamed, M. Parrinello, T. Chassaing, J. Hutter, QUICKSTEP: Fast and accurate density functional calculations using a mixed gaussian and plane waves approach, Comput. Phys. Comm. 167 (2005) 103–128.

[48] S. Nosé, A unified formulation of the constant temperature molecular dynamics methods, J. Chem. Phys. 81 (1984) 511–519.

[49] S. Nosé, A molecular dynamics method for simulation in the canonical ensemble, Mol. Phys. 52 (1984) 255–268.

[50] W. G. Hoover, Canonical dynamics: Equilibrium phase-space distribution, Phys. Rev. A 31 (1985) 1695–1697.

[51] V. I. Anisimov, J. Zaanen, O. K. Andersen, Band theory and Mott insulators: Hubbard U instead of Stoner I, Phys. Rev. B 44 (1991) 943–954.

[52] S. L. Dudarev, D. N. Manh, A. P. Sutton, Effect of Mott-Hubbard correlations on the electronic structure and structural stability of uranium dioxide, Phil. Mag. Part B 75 (1997) 613–628.

[53] S. L. Dudarev, G. A. Botton, S. Y. Savrasov, C. J. Humphreys, A. P. Sutton, Electron-energy-loss spectra and the structural stability of nickel oxide: An LSDA+U study, Phys. Rev. B 57 (1998) 1505–1509.

[54] J. VandeVondele, J. Hutter, Gaussian basis sets for accurate calculations on molecular systems in gas and condensed phases, J. Chem. Phys. 127 (2007) 114105.

[55] Y. Morino, K. Kuchitsu, A note on the classification of normal vibrations of molecules, The Journal of Chemical Physics 20 (11) (1952) 1809–1810.

[56] C. Berthomieu, A. Boussac, W. Mäntele, J. Breton, E. Nabedryk, Molecular changes following oxidoreduction of cytochrome b559 characterized by Fourier transform infrared difference spectroscopy and electron paramagnetic resonance: photooxidation in photosystem II and electrochemistry of isolated cytochrome b559 and iron protoporphyrin IX-bisimidazole model compounds, Biochemistry 31 (1992) 11460–11471.

[57] K. Hasegawa, T. Ono, T. Noguchi, Vibrational Spectra and Ab Initio DFT Calculations of 4-Methylimidazole and Its Different Protonation Forms: Infrared and Raman Markers of the Protonation State of a Histidine Side Chain, J. Phys. Chem. B 104 (2000) 4253–4265.

[58] G. Fischer, T. Tom Wydrzynski, Isotope Effects in FTIR Difference Spectra of the Photosynthetic Oxygen-Evolving Catalytic Site Determined by ab Initio Calculations on Model Compounds, J. Phys. Chem. B 105 (2001) 12894–12901.

[59] T. Noguchi, Fourier transform infrared analysis of the photosynthetic oxygen-evolving center, Coordination Chemistry Reviews 252 (2008) 336–346.

[60] L. J. Bellamy, The Infrared Spectra of Complex Molecules, Chapman & Hall, London 1 (1980) 72–96.

[61] P. Pulay, G. Fogarasi, F. Pang, J. E. Boggs, Systematic ab initio gradient calculation of molecular geometries, force constants, and dipole moment derivatives, J. Am. Chem. Soc. 101 (1979) 2550–2560.

[62] H. Chu, W. Hillier, N. A. Law, G. T. Babcock, Identification of a possible Mn-O-Mn cluster vibrational mode of the S_3 state in the oxygen-evolving complex of photosystem II by the low-frequency FTIR spectroscopy, Science Access 3 (1).

[63] L.-H. Hou, C.-M. Wu, H.-H. Huang, H.-A. Chu, Effects of Ammonia on the Structure of the Oxygen-Evolving Complex in Photosystem II As Revealed by Light-Induced FTIR Difference Spectroscopy, Biochemistry 50 (2011) 9248–9254.

[64] R. Pokhrel, G. W. Brudvig, Oxygen-evolving complex of photosystem II: correlating structure with spectroscopy, Phys. Chem. Chem. Phys. 16 (2014) 11812–11821.

[65] H. A. Chu, R. J. Debus, G. T. Babcock, D1-Asp170 is structurally coupled to the oxygen evolving complex in photosystem II as revealed by light-induced Fourier transform infrared difference spectroscopy, Biochemistry 40 (2001) 2312–2316.

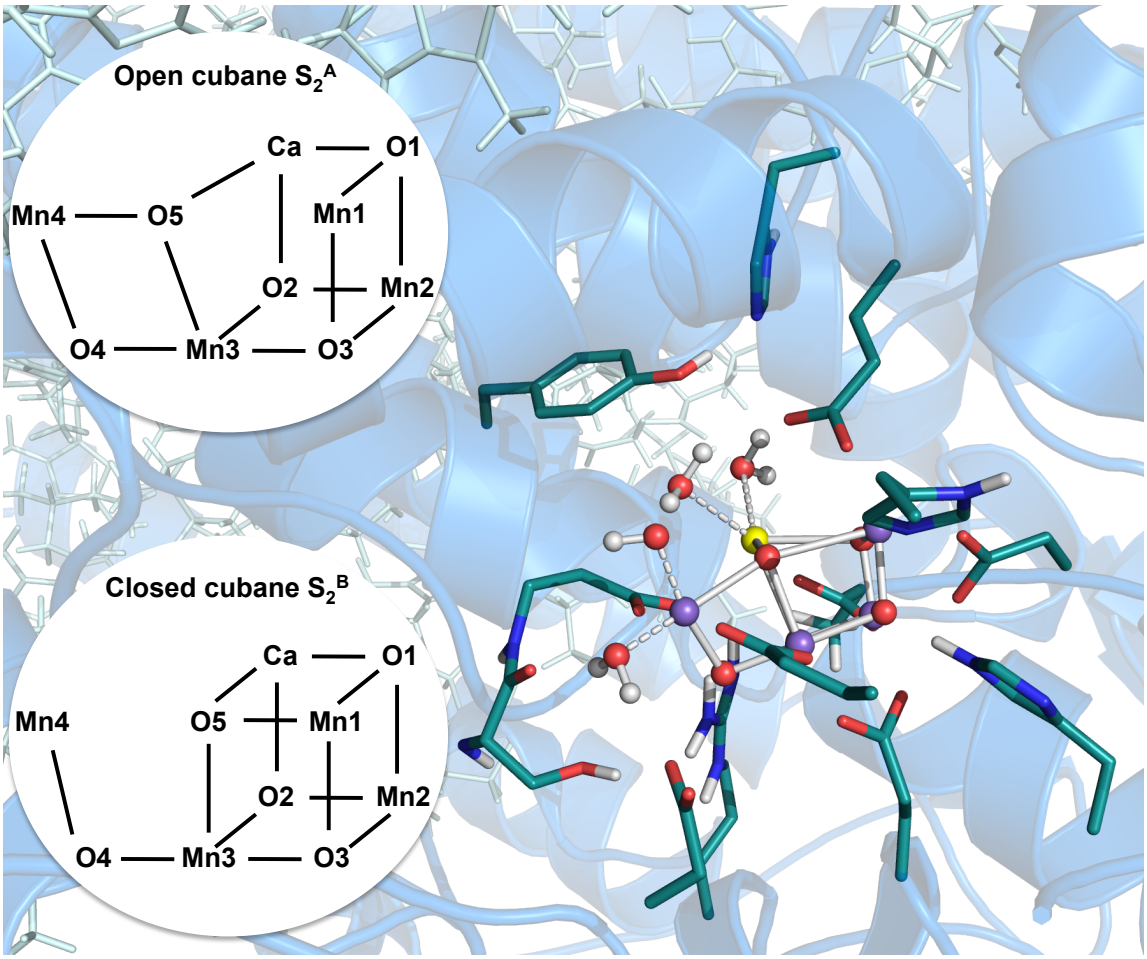

Figure 1: **Selected atoms from the molecular models of the catalytic center of the OEC used in QM/MM MD simulations.** The Mn_4CaO_5 cluster is shown by a ball-and-stick representation (Mn purple, Ca yellow, O red and H white), while the other residues included in the QM region are represented as sticks. The part of the system described at classical level is shown as cartoon (polypeptide chains) and in cyan sticks (chlorophylls). In the two insets we reported a scheme of the two conformers characteristic of the S_2 state, namely the (open cubane) S_2^A state and the (closed cubane) S_2^B state.

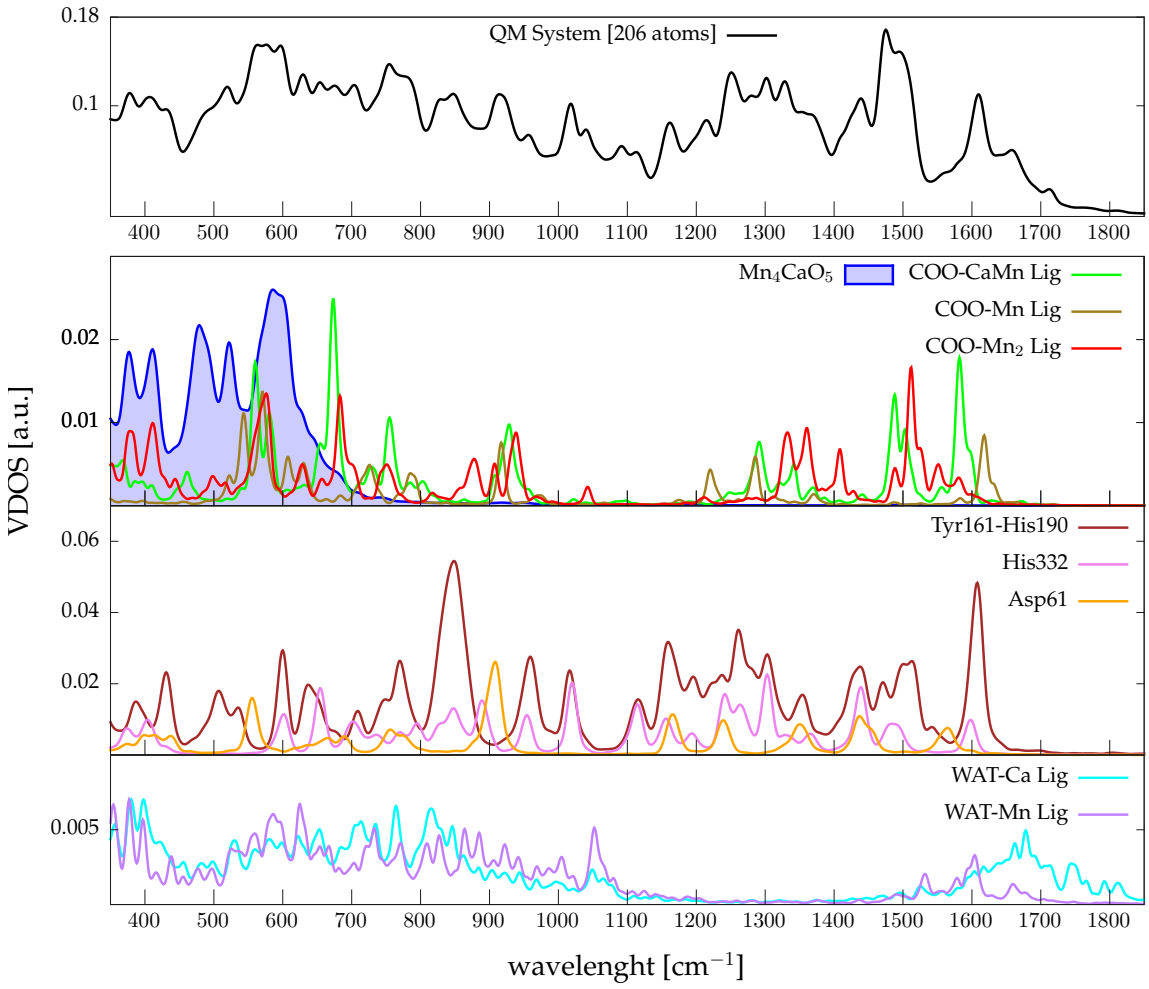

Figure 2: **Vibrational density of states spectra obtained from the QM/MM dynamics of the S_2^A state.** In each panel the VDOS spectrum is calculated on restricted sub-system of selected atoms as reported in the legends. The black line accounts for the entire quantum system (206 atoms).

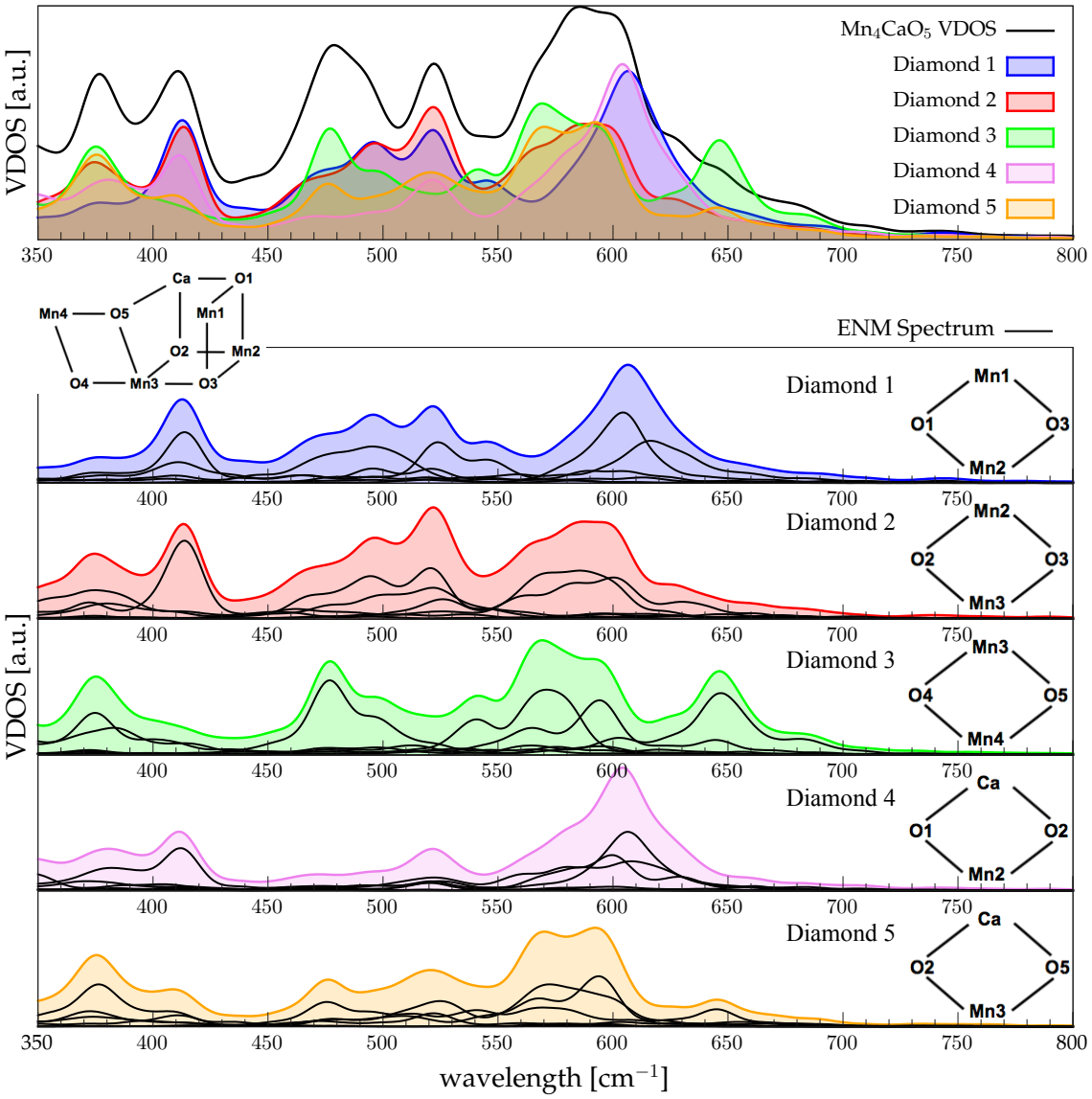

Figure 3: **Effective Normal Modes Analysis of the Mn_4CaO_5 cluster (10 atoms in the sketch) from the QM/MM dynamics of the S_2^A state.** In the upper panel the VDOS spectrum of the Mn_4CaO_5 cluster is reported together with the VDOS calculated on the internal coordinates of the five diamond groups composing the cluster defined on the right side of the panel. In the bottom panel, for each diamond group, we report the overall spectra of the group as well as its decomposition in the contribution of internal collective modes, calculated using the effective normal modes analysis.

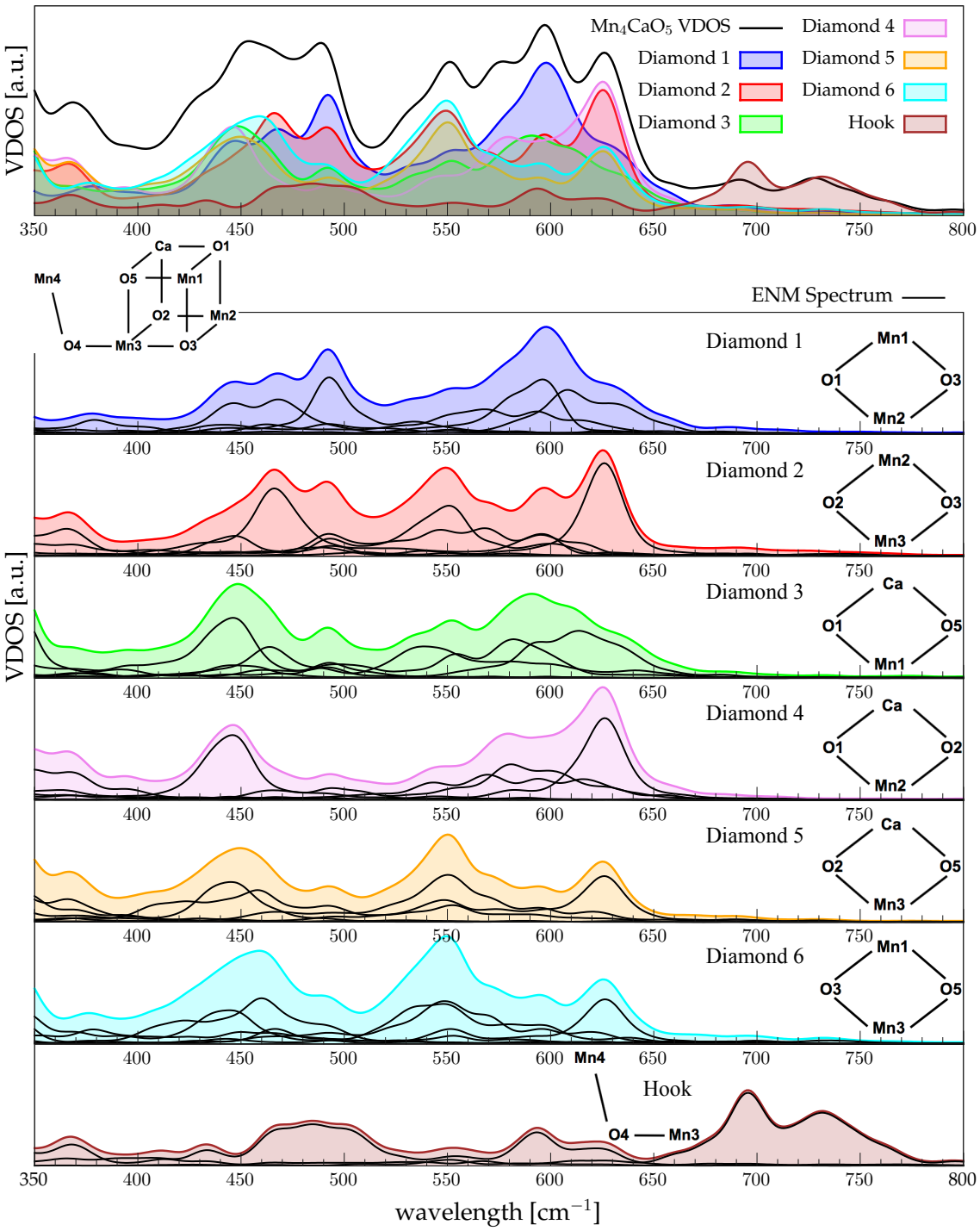

Figure 4: **Effective Normal Modes Analysis of the Mn_4CaO_5 cluster (10 atoms in the sketch) from the QM/MM dynamics of the S_2^B state.** In the upper panel the VDOS spectrum of the Mn_4CaO_5 cluster is reported together with the VDOS calculated on the internal coordinates of the five diamond groups plus the hook group (i.e. the group associated to the dangling manganese ion) composing the cluster and defined on the right side of the panel. In the bottom panel, for each group, we report the overall spectra of the group as well as its decomposition in the contribution of internal collective modes, calculated using the effective normal modes analysis.

Mode Description	Frequency [cm^{-1}]
OPEN CUBANE	
Mn3-O4	647
Mn1-O1-Mn2 Asym	617
Mn2-O1	604
Mn2-O2	600
Mn3-O5	594
Mn3-O2	572
O4-Mn4-O5 Sym	571
Mn1-O3-Mn2 Sym	524
Mn1-O3-Mn2 Asym	495
O4-Mn4-O5 Asym	477
Mn2-O3-Mn3 Asym	414
CLOSED CUBANE	
Mn3-O4	696
Mn2-O2	626
Mn1-O1	608
Mn1-O3	595
Mn1-05 + Mn2-O1	581
Mode mix of Mn3	550
O1-Mn2-O3 Sym	493
Mn3-O4-Mn4 Sym	485
Mn2-O3-Mn3 Asym	466
Mn1-O5-Mn3 Asym	461

Table 1: **Identification of specific vibrational modes of the Mn_4CaO_5 cluster in the S_2^A and S_2^B models.** The characterization is performed on the basis of the effective normal modes analysis.